Efficiency Comparison of Large-Scale Standalone, Centralized, and Distributed Thermochemical Biorefineries

Efficiency Comparison of Large-Scale Standalone, Centralized, and Distributed Thermochemical Biorefineries

Alberto Alamia,*[a] Stefania Òsk Gardarsdòttir,[a] Anton Larsson,[a, b] Fredrik Normann,[a] and Henrik Thunman[a]

We present a comparison of three strategies for the introduction of new biorefineries: standalone and centralized drop-in, which are placed within a cluster of chemical industries, and distributed drop-in, which is connected to other plants by a pipeline. The aim was to quantify the efficiencies and the production ranges to support local transition to a circular economy based on biomass usage. The products considered are biomethane (standalone) and hydrogen/biomethane and sustainable town gas (centralized drop-in and distributed drop-in). The analysis is based on a flow-sheet simulation of different process designs at the 100 $MW_{biomass}$ scale and includes the following aspects: advanced drying systems, the coproduction of ethanol, and power-to-gas conversion by direct heating or water electrolysis. For the standalone plant, the chemical efficiency was in the range of 78–82.8 % $LHV_{a.r.50\%}$ (lower heating value of the as-received biomass with 50 % wet basis moisture), with a maximum production of 72 MW_{CH_4}, and for the centralized drop-in and distributed drop-in plants, the chemical efficiency was in the range of 82.8–98.5 % $LHV_{a.r.50\%}$ with maximum production levels of 85.6 MW_{STG} and 22.5 MW_{H_2}/51 MW_{CH_4}, respectively. It is concluded that standalone plants offer no substantial advantages over distributed drop-in or centralized drop-in plants unless methane is the desired product.

Introduction

The transition towards a circular economy that is based on biomass products requires the introduction of new biorefineries that respect the targets set in terms of sustainability and economic growth. In particular, thermochemical biorefineries based on the gasification of lignocellulosic biomass and waste can combine a large-scale production with a high conversion efficiency.[1–3] The development of gasification technology over the last few decades has resulted in several demonstration plants (1–32 $MW_{biomass}$)[4–9] with efficiencies from biomass to final product in the range of 50–65 % lower heating value dry ash-free (LHV_{daf}). However, to propel the desired breakthrough of biomass-based products it is necessary to improve the profitability levels of these plants, through the increase of the plant size and efficiency and by identifying economically viable opportunities for the chemical, transport, and energy sectors.

The strategies to be used for the introduction of new gasification plants are not only influenced by the local energy market (prices of feedstock and products) but also by the inherent trade-off between the economy of scale and the logistics of biomass for the plant. In particular, the investment cost for the handling and preparation (which includes drying) of the feedstock is considerable because of the low energy density and high moisture content of the fresh biomass.[10–12] Therefore, the profitability of new plants is affected by the availability of existing infrastructure for biomass handling and of other heat sources for drying, for example, waste heat from existing industrial sites.

The strategies to be applied for the introduction of biomass gasification plants, which are highly dependent upon regional conditions, fall into three main groups: standalone, which produces biofuel or chemicals; centralized drop-in, for a cluster of chemical industries; and distributed drop-in, which involves a connection to a network of chemical plants (Figure 1). Standalone plants[12–16] have their own biomass handling and product distribution facilities, which entail either a pipeline (e.g., biomethane) or a truck/ship (other biochemicals). In contrast to the standalone plants, centralized drop-in plants[17–19] serve a low number of customers located closely (i.e., a cluster of industries) with an intermediate product, which can substitute a fossil equivalent at the customer's site directly. Typically, this intermediate is a nitrogen-free gas with a composition that varies from pure H_2, which is highly desirable for chemical plants based on oil, to

[a] A. Alamia, S. Òsk Gardarsdòttir, Dr. A. Larsson, Dr. F. Normann, Prof. H. Thunman
Division of Energy Technology
Chalmers University of Technology
Hörsalsvägen 7, 412-96, Gothenburg (Sweden)
E-mail: alamia@chalmers.se

[b] Dr. A. Larsson
Göteborg Energi AB
Fågelrovägen 16, 418 34 Gothenburg (Sweden)

The ORCID identification number(s) for the author(s) of this article can be found under http://dx.doi.org/10.1002/ente.201600719.

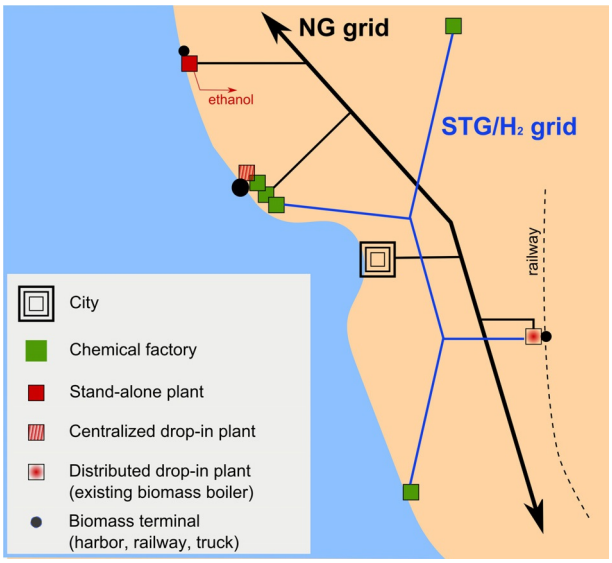

Figure 1. Differences between the three different implementation strategies for biomass gasification, that is, the standalone, centralized drop-in, and distributed drop-in gasification plants.

a mixture of H_2 and CO, and CO_2, which may also include significant amounts of CH_4 and other hydrocarbons. The distribution pressure is moderate (10–20 bar) so that gases with high dew-points and a significant fraction of CO_2 can be transported. This reduces the complexity of the centralized drop-in gasification plant compared to that of a standalone plant as the final product upgrade is performed by the existing equipment at the premises of the costumer. Further synergies can be achieved by, for example, integrating the steam cycle or utilizing existing methane reformers. However, an infrastructure for biomass handling (storage, drying, transport terminal, etc.) is often missing and needs to be built on an ad hoc basis. Distributed drop-in gasification plants are not integrated physically with the synthesis process at the customer's site but instead produce a nitrogen-free, intermediate product for distribution through a regional pipeline (Figure 1), herein termed "sustainable town gas" (STG). The main advantage of distributed drop-in plants is the possibility to build them at locations favorable for biomass logistics, that is, easily accessible by road, railway, and ship. In particular, existing biomass boilers and pulp mills have the required infrastructures (biomass handling, steam cycles, heat recovery network, and in many cases even dryers) to achieve a high performance through retrofitting or upgrading to gasification plants, although they lack a pipeline connection to the customers' plants. Another potential advantage of decentralization is the redundancy of the regional STG/H_2 pipelines with respect to the national gas grid, which offers flexibility to consumers in terms of seasonal variations of prices and the production of gasification-based products.

We present an analysis of proposed process designs for standalone, centralized drop-in, and distributed drop-in plants with the aim to quantify their efficiencies and production ranges. The results are intended to support the formulation of local strategies for the introduction of gasification processes as part of the transition to a circular economy. The evaluation was performed using process simulations in Aspen Plus based on the design of the GoBiGas plant,[7,20–22] which produces biomethane (also referred to as synthetic natural gas, substitute natural gas, or SNG) from biomass on a commercial scale and represents the state-of-the-art technology for highly efficient gasification.

Methodology

We focus initially on the evaluation of the state-of-the-art standalone biomethane plant operated on a commercial scale, with the introduction of a series of proposed improvements to the process. In the second phase of the study, process designs for distributed drop-in and centralized drop-in plants are analyzed and compared to those for standalone plants with a focus on the achievable efficiencies and product ranges. The process design for the standalone plant was based on that of the GoBiGas plant[7,20,22,23] in Gothenburg, Sweden, which is currently the largest plant in the world that combines biomass gasification technology and methane synthesis. The GoBiGas plant was constructed in 2014 as a demonstration plant with a capacity of 32 $MW_{biomass}$ (20 $MW_{biomethane}$) based on the lower heating value (LHV) of dry ash-free biomass and it uses predried feedstock.[22] The biomethane produced has a methane content $>96\,\%_v$, which is injected into the national natural gas grid. In this investigation, a plant size of 100 $MW_{biomass}$ is used as the reference, in which 100–300 $MW_{biomass}$ would be considered optimal for commercial gasification plants.[24,25] The feedstock has a moisture content of 40 % on a wet basis (w.b.) and the effects of dryers (not included in the GoBiGas design) that are integrated with the heat recovery network and steam cycle are analyzed.

Other aspects investigated for the standalone strategy were: (i) the possibility to introduce power-to-gas technologies to increase the production of methane; and (ii) the coproduction of methane and ethanol. Power-to-gas technologies are of interest because electricity can be added intermittently to a continuous production process, which thereby enables conversion from intermittent renewable energy sources.

Furthermore, the surplus of electricity generated from the excess heat in the process can be converted to methane to recirculate energy in the process. Two power-to-gas technologies were investigated: a traditional process based on the electrolysis of water and the direct heating of the gasifier to reduce char combustion.[22] The coproduction of methane and ethanol was considered as ethanol is the main drop-in alternative to gasoline on the market. The biochemical pathway (syngas fermentation) to ethanol was selected as it offers a high efficiency, tolerates sulfur impurities in the syngas (in contrast to metallic catalysts), and is less affected by inert gases, such as methane. Furthermore, the production technology has recently reached the stage of maturity necessary for industrial applications.[26,27]

The high-energy demand for distillation is a key issue to achieve a high efficiency for ethanol production, and the

direct integration of the distillation process into the rest of the plant would lead to an overall low efficiency as extensive streams with high exergy would be used to meet a demand that could instead be achieved using a low-exergy stream. However, the water/ethanol mixture can be stored in regular tanks, which provides an opportunity to use the distillation process to balance the load of other low-temperature heat sources, for example, a district heating plant, or to balance the electricity demand within the grid. This confers advantages upon the local/regional energy system that can motivate the production of ethanol.

In the investigation of centralized drop-in and distributed drop-in plants, two possible nitrogen-free intermediate products are considered: STG, that is, upgraded syngas from biomass gasification, and hydrogen. The major difference between the two intermediates is the presence in the STG of CH_4 (5–15 $\%_v$), which is a typical product of biomass gasification. As chemical factories reform CH_4 to syngas, its production during gasification is rather a penalty than a benefit, contrary to that in the biomethane process. However, the reforming of renewable methane is questionable as it is a valuable product on the biofuel market. Therefore, the two intermediates taken into consideration represent two extreme choices: (i) STG for supply to industries already equipped with a natural gas reformer and (ii) hydrogen obtained by separation (coproduction) in the biomethane process. The separation of hydrogen in the biomethane process was investigated by using vacuum pressure swing adsorption (VPSA). Both intermediate products can be produced by distributed drop-in and centralized drop-in plants, although STG is considered more suitable for distributed production and distribution because of its lower energy demand for compression.

Investigated designs and system boundaries

We focus on four design classes (Figure 2 and Table 1). The classification is based on the final product of the process. Designs of class A produce biomethane, class B designs produce methane and ethanol, class C designs produce methane and/or STG, and class D designs produce biomethane and hydrogen. The process analysis includes the gasification and gas synthesis as well as the steam cycle for heat recovery and electricity production, which is not included in the current GoBiGas process. The outline of the gasification plant and methane synthesis are common to all the designs and are based on the layout of the GoBiGas plant (outlined in black in Figure 2 and described in greater detail in a later section). Briefly, the gasification plant includes a gasification section that is based on dual fluidized bed (DFB) technology and tar removal stages, and the produced syngas is subsequently compressed and delivered to the premethanation section or to the STG grid (Figure 2c). In the premethanation section, the gas undergoes further cleaning steps (hydrogenation of olefins, removal of H_2S and CO_2), a water gas shift (WGS)

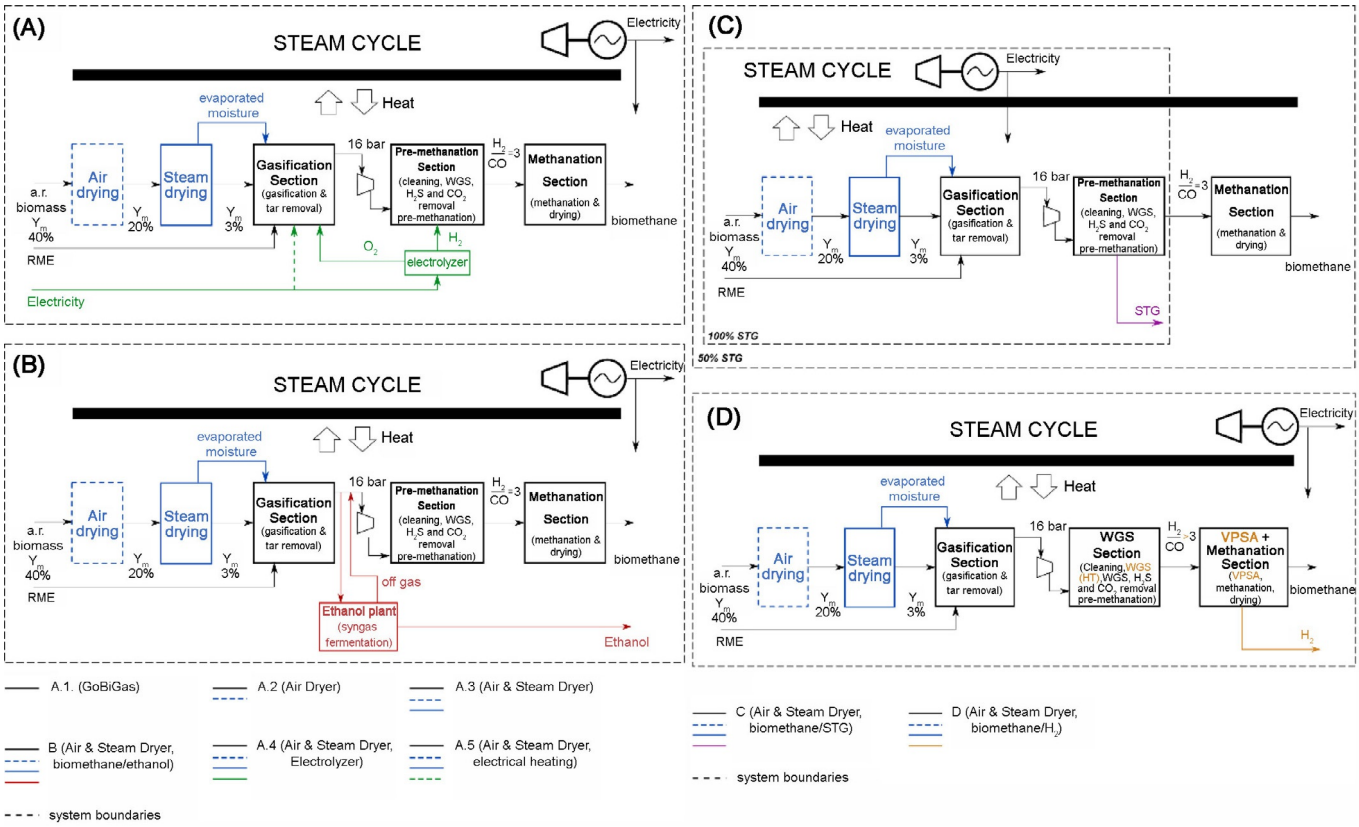

Figure 2. a, b) Designs A.1–5 for a standalone biomethane plant and design B for a plant with the coproduction of ethanol. c, d) Designs C and D for the coproduction of STG/biomethane and H_2/biomethane, respectively, in a distributed/centralized drop-in plant.

Table 1. Designs of the plants used in the present investigation.

Design	Product 1	Product 2	Strategy	Networks	Power-to-gas	Drying
A.1	biomethane	–	standalone	NG[a], electricity	no	none
A.2	biomethane	–	standalone	NG, electricity	no	single-stage[b]
A.3	biomethane	–	standalone	NG, electricity	no	double-stage[c]
A.4	biomethane	–	standalone	NG, electricity	electrolysis	double-stage[c]
A.5	biomethane	–	standalone	NG, electricity	direct heating	double-stage[c]
B	biomethane	ethanol	standalone	NG, electricity, ethanol	no	double-stage[c]
C	STG	biomethane[d]	centralized/ distributed	STG, electricity, NG[d]	no	double-stage[c]
D	hydrogen	biomethane	centralized/distributed	hydrogen, NG, electricity	no	double-stage[c]

[a] NG: natural gas. [b] Air-drying. [c] Air- and steam-drying with moisture recovery as the gasification agent. [d] Optional.

reaction, and an initial premethanation reaction. In the final methanation section, the syngas is converted fully to methane in a four-stage direct methanation process and then dried to achieve a methane content $>96\,\%_v$. The modifications made to the other designs are highlighted in color (Figure 2a–d).

A detailed list of the investigated designs is given in Table 1. Compared to the GoBiGas design A.1, design A.2 includes additional air-drying of the fuel[28] in which the moisture content is reduced from 40 to 20% w.b. Design A.3 includes additional air-drying, complemented with a steam dryer that recovers the evaporated water as a gasification agent (which thereby reduces the steam demand for the gasifier). Design A.3 is used as the base case for the standalone biomethane plant and for the distributed/centralized drop-in plants. Designs A.4 and A.5 evaluate two power-to-gas concepts. The first concept includes an electrolyzer that feeds hydrogen to the syngas in the premethanation section (A.4). In the second design concept, the gasifier is heated electrically (A.5). The power-to-gas designs can use both the electricity produced from the excess heat in the plant and electricity derived from intermittent energy sources (wind and solar) and drawn from the grid.

The maximum production level of ethanol is obtained by considering the entire syngas flow, although the production can be shifted towards methane, which thereby bypasses the fermentation plant. A similar approach is applied in design C, in which STG is produced in a distributed/centralized drop-in plant (Figure 2c). Design D is used to investigate the coproduction of biomethane and hydrogen by the VPSA separation upstream of the final methanation step. In this case, an additional WGS reactor is introduced at high temperature (400 °C) to maximize the production of hydrogen.

Process layout and modeling

The process simulations were performed by using Aspen Plus using hierarchy blocks with submodels of different process equipment and Fortran routines. The flow-sheet model has been validated against data from the GoBiGas plant[7,22] (Table 2), together with additional measurements brought forward to this work (see later, Table 4). The heat integration in the plant is evaluated and optimized by applying a pinch analysis,[30] in which the heat recovery network is complemented with biomass dryers and a steam cycle for the production of electricity. The overall property method used, unless stated otherwise, is the Peng–Robinson equation of state with Boston–Mathias modification.

Table 2. Experimental data from the GoBiGas plant (gasification section).

DFB gasifier	HT	LT
gasifier bed temperature [°C]	870	820
raw gas temperature [°C]	815	800
combustor temperature [°C]	920	870
max. steam temperature [°C]	550	550
maximum air temperature [°C]	550	550
flue gas temperature [°C]	140	140
fluidization steam [$kg\,kg_{daf}^{-1}$]	0.5	0.5
stoichiometric ratio combustor	1.2	1.2
purge gas (CO_2) flow [$kg\,kg_{daf}^{-1}$]	0.1	0.1
gas composition	HT	LT
H_2 [$vol\,\%_{dry}$]	42.1	39.9
CO [$vol\,\%_{dry}$]	24.1	24.0
CO_2 [$vol\,\%_{dry}$]	23.5[a]	25.3[a]
CH_4 [$vol\,\%_{dry}$]	8.6	7.7
C_2H_2 [$vol\,\%_{dry}$]	0.13	0.13
C_2H_4 [$vol\,\%_{dry}$]	2.0	1.9
C_2H_6 [$vol\,\%_{dry}$]	0.19	0.19
C_3H_6 [$vol\,\%_{dry}$]	0.001	0.001
H_2O [vol%]	6.3[b]	6.3[b]
total tar [$g\,Nm^{-3}$]	10	20.5
BTX [$g\,Nm^{-3}$]	3	7

[a] net of the purge gas; [b] saturated

Process design based on GoBiGas

The layout of design A.1 (GoBiGas) is presented in Figure 3, and all the experimental data used in the simulations are reported in Figure 3 and Tables 2 and 3. The submodel used for the DFB gasifier is based on a previous study[29] in which experimental data (Table 3) were used to calculate a set of fuel conversion variables that describe the gasification and combustion processes. The experimental data are taken from a previous evaluation of the GoBiGas gasifier[22] with full closure of the mass balance, and with an operation range that varies between two operating conditions: high-temperature (HT) operation with gasification at 870 °C and a tar content of 10 $g\,Nm^{-3}$; and low-temperature (LT) operation with gasification at 820 °C and a tar content of 20.5 $g\,Nm^{-3}$. The

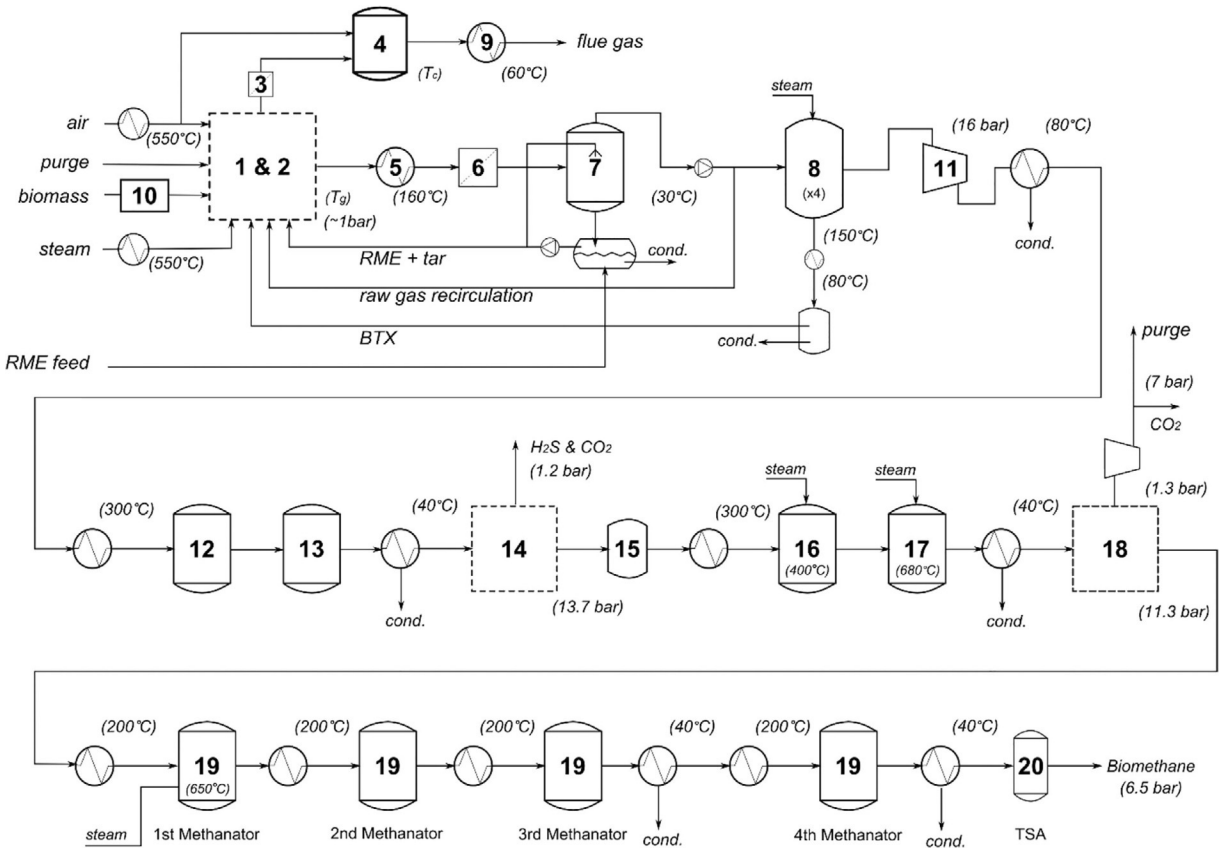

Figure 3. Process flow-sheet of the GoBiGas design at 100 $MW_{biomass}$. Designations: 1 gasifier (separate DFB submodel)[29]; 2 combustor (separate DFB submodel); 3 cyclone; 4 postcombustion chamber; 5 raw gas cooler; 6 raw gas filter; 7 RME scrubber; 8 carbon beds; 9 flue gas train; 10 fuel feeding system; 11 product gas compressor; 12 olefins hydrogenator; 13 COS hydrolyzer; 14 H_2S removal (separate submodel); 15 guard bed; 16 WGS; 17 premethanation; 18 CO_2 removal (separate sub-model); 19 methanation; 20 TSA drying.

fuel conversion variables include char gasification X_g, oxygen transport, and the fraction of volatile matter that is converted to each of the energy-carrying compounds of the raw gas. One advantage of this approach is that the heat balance can be extrapolated for different conditions.[22,29] This method enables the transfer of experimental knowledge from smaller facilities to a larger plant, which can differ with respect to heat losses, preheating of ingoing streams, moisture content of the feedstock, and other parameters that affect the efficiency of the process. Compared to the GoBiGas plant (32 $MW_{biomass}$), the heat balance in the flow-sheet (100 $MW_{biomass}$, design A.1) is modified to account for the preheating of the steam and air to a higher temperature (550 °C instead of the 350 °C used in the current operation) and reduced heat losses, from 5.2% of the energy in the fuel[22] (current design) to 0.5–2.5%, compared to the heat losses of the circulating fluidized bed (CFB) boilers of a relevant size.[31]

The flue gas from the combustion side of the DFB gasifier is directed to a postcombustion chamber (**4** in Figure 3), which is then used to combust the off-gases and slipstreams. The sensible heat in the flue gases is then recovered through heat exchange (**9**). The raw gas produced is cooled (**5**), and any particles are removed by passing through a textile-bag filter (**6**), before it enters the tar scrubber (**7**). A continuous flow of rape methyl esters (RME) is fed into the scrubber to avoid saturation by naphthalene, which is the main tar component removed in this stage. The used RME and the extracted tar are fed to the combustor to provide additional heat to the gasification process.

Downstream of the scrubber, a fan controls the gas flow through the gasifier and enables the recirculation of raw gas to the combustor, which thereby provides extra heat to the gasification process if necessary. A minimum level of recirculation of the raw gas is required to stabilize the temperature in the gasification system and to cope with fluctuations in the moisture content of the fuel. Light cyclic hydrocarbons, mainly benzene and small fractions of toluene and xylene (referred to as BTX) remain in the gas at this point and they are removed in the subsequent section through a series of three fixed beds that are filled with active carbon. The plant has four active carbon beds (**8**), which enable the steam regeneration of one bed at all times. The off-gases from the regeneration are condensed to recover heat, and the extracted tar compounds are fed to the combustor. Notably, for large plants, a scrubber might be a suitable alternative to the carbon beds, although this issue is outside the scope of the present study.

The syngas derived from the gasification requires further cleaning and shift stages to achieve the level of purity and

Table 3. Data from GoBiGas plant (tar removal and H_2S and CO_2 removal sections).

Tar cleaning		
cooler temperature [°C]	160	
maximum tar content in raw gas [g Nm^{-3}]		25
fresh RME flow [MW_{RME}/MW_{fuel}]		3.0
temperature of RME scrubber [°C]		35
average flow of steam to carbon bed [kg kg_{BTX}^{-1}]		9.2
temperature of steam to carbon beds [°C]		250
pressure of steam to carbon beds [bar]		3.8
amine processes	H_2S removal	CO_2 removal
absorber pressure [bar]	13.7	11.3
stripper pressure [bar]	1.2	1.3
solvent concentration in CO_2-unloaded solution, MDEA/PZ [wt%]	37.5/0	35.2/6.3
lean solvent loading [mol_{CO_2} $mol_{solvent}^{-1}$]	0.02	0.28
heat requirement for solvent regeneration [MJ $kg_{CO_2}^{-1}$]	2.24	0.83
electricity requirement [MW]	0.05	0.09
cooling requirement [MW]	4.09	2.37
H_2S removal rate [%]	59	–
H_2S concentration in clean gas [ppm]	0.01	–
CO_2 removal rate [%]	56	95
CO_2 concentration in clean gas [$\%_v$]	13.8	2.5
CO_2 final pressure [bar]	1.2	7

composition required for the final synthesis of methane. The pressure in the premethanation section is increased to 16 bar through a six-stage intercooled compressor to meet the requirements for the hydration of olefins and COS (carbonyl sulfide) in reactors **12** and **13**. Notably, the pressure level is not set by the methanation stages, as assumed in some previous studies. The subsequent cleaning steps include the H_2S (**14**) and CO_2 (**18**) separation processes, which rely on selective chemical absorption using amines under pressurized conditions, in which methyl diethanolamine (MDEA) is used in the former process and a MDEA + piperazine (MDEA + PZ) mixture is used in the latter.

The high pressure in the premethanation section is decreased partially in the CO_2 separation stage (Figure 4) to reduce the heat consumption in the reboiler significantly (Table 3).The simulation of the H_2S and CO_2 separation processes is performed separately in two submodels using a rate-based approach, the Aspen Plus built-in electrolyte NRTL method and the Redlich–Kwong equation of state to compute liquid- and vapor-phase properties, respectively. The absorption and stripper columns are modeled as multistage packed columns that use the IMTP™ packing material. The compositions of the solvents and the energy input for solvent regeneration are based on data obtained from the GoBiGas plant.

The removal of the H_2S is modeled according to the work of Bolhàr-Nordenkampf et al.[32] who used a standard absorber–desorber setup with a lean–rich solvent heat exchanger between the columns. The submodel for CO_2 removal (Figure 4) is based on the layout of the GoBiGas plant and includes standard process units as well as additional two-

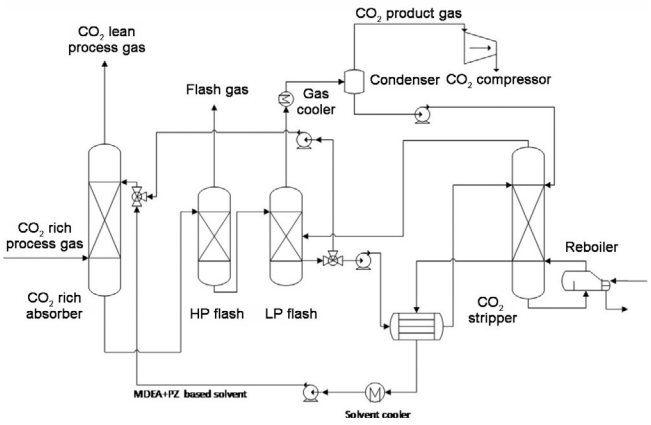

Figure 4. Submodel for the separation of CO_2.

stage flashing of the CO_2-rich solvent between the absorber and the cross-heat exchanger. The CO_2 removed in the first scrubber-absorber is contaminated with H_2S, whereas that removed during the second process is of higher purity and is compressed to 7 bar for use as a purge gas. Both CO_2-containing streams are suitable for use in carbon capture and storage (CCS), which would create a negative CO_2 impact for the use of this biomass.

The gasification plant has the potential to become a carbon-negative facility by combining bioenergy with carbon capture and storage (BECCS).[33] BECCS requires additional on-site compression to 70–110 bar for the transportation and storage of the CO_2.[34] CO_2 storage for climate mitigation is a clear use for the separated CO_2, so the concept of BECCS has been discussed as a promising tool to attain stringent climate mitigation targets.

A guard bed (**15**) is located upstream of the reactors with a sulfur-sensitive catalyst to protect it from possible contamination. The WGS reactor (**16**) is operated at approximately 300 °C, and the H_2/CO ratio is increased from the original value of approximately 1.7 to the optimal value for the synthesis of methane of >3. Thereafter, the syngas is directed to a premethanation reactor, in which some of the CO and CO_2 is converted to CH_4 (**17**) and the C_2 and C_3 hydrocarbons are cracked; as these reactions are strongly endothermic, and the temperature increases to around 680 °C. The methanation process (**19**) is a proprietary Haldor Topsøe technology named TREMP,[35] which is based on the MCR methanation catalyst. The main characteristic of this system is the high temperature increase allowed in a single reactor (up to 500 °C[36]), which results in a very low (or zero) recycle ratio. The fixed-bed design of the reactors enables the recovery of excess heat in the form of high-pressure superheated steam. In the GoBiGas plant (Figure 3), four methanation reactors without recycling are applied, followed by a final drying stage based on temperature swing adsorption (TSA), which then meets the purity target (>96 $\%_v$ methane, <0.5 $\%_v$ CO, <1 $\%_v$ H_2). The methanation reactors are simulated as Gibbs reactors with a maximum temperature in the first stage of <680 °C. Steam is added before the first methanation stage

to avoid carbon formation on the catalyst. The final product is delivered at 6.0–6.5 bar to the compression station (not included in the process analysis), in which the pressure is once again increased to 30 bar to enable injection into the natural gas network.

Additional modeling of process equipment

Dryers

The modeling of the air dryer is based on the work conducted by Holmberg and Ahtila,[28] which involves single-stage drying without recycling, and the modeling of the steam dryer follows the work of Alamia et al.[37] The steam-drying is divided into three stages with steam temperatures of 150, 120, and 150 °C to dry and preheat the biomass. The concept enables a moisture content of <5 % w.b. with the extraction of the evaporated moisture in the final two stages to yield a final moisture temperature of around 150 °C. The moisture recovery corresponds to a saving of 0.2–0.25 $kg_{H_2O}\,kg_{daf}^{-1}$ of the gasification steam (drying from 20 to 3–5 % w.b.), which represents approximately half of the steam used in the DFB gasifier. The specific work consumption is calculated from the results of the CFD and Aspen simulations of the dryer, as presented previously[37] (Table 4).

Power-to-gas

Power-to-gas processes based on electrolysis are commercially available.[38–40] In a biomethane plant, electrolysis is operated at 10 bar, and the hydrogen is injected after the WGS reactor to adjust the H_2/CO ratio before methanation. Compared to the standalone electrolysis processes, integration in a biomethane plant is particularly favorable because of the existing methanation reactor and the renewable CO and CO_2 already present in the syngas, which otherwise would have to be obtained from other processes. Furthermore, the oxygen can be used in the combustor to reduce the inlet air flow, so the only equipment required is the electrolyzer. In the flowsheet model, the electrolyzer is simulated from data obtained previously with regard to the alkaline electrolyzer[41] module of 3.5 MW_{el} electrical capacity, based on the original Lurgi technology.[42] This represents the state of the art in large-scale alkaline electrolyzers and it is currently used in several plants. The input data used in the simulations are summarized in Table 4. The heat released during the electrolysis process is not accounted for in the pinch analysis because of the low outlet temperature of the cooling stream (<50 °C) associated with the current design of the unit. A retrofit of the current design of the electrolyzer is outside the scope of this work. To calculate the range of operation of the electrolysis process, two cases are investigated: $zero_{El}$, in which only the electricity produced in the plant is converted; and the maximum electricity case (max_{El}), in which electricity from the grid is used to achieve the H_2/CO ratio for methanation without a WGS reactor.

Table 4. Literature data for modeling.

System and parameters	Data
air dryer[28]	
air temperature [°C]	95
specific heat consumption [kJ $kg_{H_2O}^{-1}$]	2900–2750
specific work consumption [kJ $kg_{H_2O}^{-1}$]	20–150
recirculation rate [%]	0–15
steam dryer: three stages[37]	
steam temperatures [°C]	150, 120, 150
specific heat consumption [kJ $kg_{H_2O}^{-1}$]	2310
specific work consumption [kJ $kg_{H_2O}^{-1}$]	352
final biomass temperature [°C]	112
recovered moisture temperature [°C]	150
syngas fermentation[26,27,44–46]	
inlet pressure [bar]	1.8[26]
makeup process water [t t_{eth}^{-1}]	8.5[26]
overall CO conversion [%]	50[44]–80[45]
overall H_2 conversion [%]	45[44]–75[45]
char gasification	
char gasification range [%]	40–70
electrolyzer[41]	
pressure [bar]	10
electricity consumption [kWh $Nm_{H_2}^{-3}$]	4.5
VPSA[47]	
syngas inlet pressure [bar]	13.2
pressure drop of H_2 [bar]	0.1
pressure ratio of CH_4-rich gas	16.5
compression of CH_4-rich gas [bar]	7.5
H_2 recovery [%]	75–95 (max)
high-temperature WGS [°C]	400
steam cycle	
steam pressure [bar]	100
steam temperature [°C]	580
cold utility temperature [°C]	15
minimum vapor fraction in turbine	0.88
number of pressure levels in the plant	2–5
ΔT_{min} [°C]	5–10
turbine isentropic efficiency	0.78–0.93

Power-to-gas conversion through the direct heating of the DFB gasifier can be achieved by introducing a resistance heater into the DFB gasifier or by further preheating the inlet gases.[22] The effect is a reduction of the internal heat demand of the gasifier, which thereby reduces char combustion and increases char gasification. The main advantage of this process over electrolysis is its higher efficiency as almost all the electricity provided is stored in the forms of gasification products and it has lower investment costs. A technical limitation of this technology is the maximum gasification of char that results from the conversion of biomass in the gasifier. This is limited arbitrarily to 70 % in the simulations based on the current gasification level in the GoBiGas plant (≈54 %[22]) with the assumption that it can be increased by optimizing the reactor design, the catalytic effects of the ash compounds,[20,43] and the heat balance in the DFB reactors. The range of operation is calculated by investigating the $zero_{El}$ case and the maximum gasification case max_{El}.

Ethanol fermentation

Ethanol can be produced by syngas fermentation[27,45,48,49] that uses fermenting organisms that have high tolerances for contaminants, such as sulfur and some tar compounds. The modeling of the fermentation process is based on the LanzaTech design for the steel-manufacturing industry as it currently is the most advanced design in terms of scale reported previously and is already in production in two plants in China,[26,46] with an output capacity of 300 tonnes per year (0.35 MW).[46] The technology used for fermentation to produce syngas from gasification was recently (May 2016) acquired by Aemetis, which is planning the construction of a plant with a capacity of 24 tonnes per year, to be completed in 2017, followed by expansion to 96 tonnes per year.[50] In the LanzaTech process, the syngas is introduced into the bioreactor and mixed with the liquid medium that contains the biocatalyst (the bacterium *Clostridium autoethanogenum*), which is consumed throughout the reactor. The product at the outlet of the reactor is directed to the steadfast separation system (which includes distillation), which recycles the liquid that contains the microorganisms to the bioreactor and separates the main product from the byproducts.[26] As the information available from the process manufacturers is limited, the flow-sheet simulation (Figure 5) is modeled by introducing data from other studies [Eqs. (1)–(4)].

$$4\,CO + 2\,H_2O \rightarrow CH_3COOH + 2\,CO_2 \quad (1)$$

$$4\,H_2 + 2\,CO_2 \rightarrow CH_3COOH + 2\,H_2O \quad (2)$$

$$6\,CO + 3\,H_2O \rightarrow C_2H_5OH + 4\,CO_2 \quad (3)$$

$$6\,H_2 + 2\,CO_2 \rightarrow C_2H_5OH + 3\,H_2O \quad (4)$$

The fermentation process is simulated with a stoichiometric reactor using reactions (1)–(4). The conversion rates of CO and H_2 in the process are set at 50 and 45 %, respectively, according to previous data from studies with a gas that has a similar H_2/CO ratio.[27,44,51,52] However, higher conversion rates (c; for CO, 80 %; and for H_2, 75 %) can be achieved through extensive recycling.[45,46] As a result of a lack of published data, two cases are simulated ($c_{80\,\%}$ and $c_{50\,\%}$ in the results) to cover the whole range. The concentration of ethanol in the outlet liquid has not been reported for the demonstration units, which creates uncertainty with regard to the estimate of the distillation energy. Here, the final concentration of ethanol is set within the range of values reported previously: from 0.5[27] to 48 g L^{-1}.[53] The distillation energy is not accounted for in the analysis of the plant as other low-temperature energy sources can be involved and this would require a dynamic analysis of the local/regional system, which is outside the scope of this work. For this reason, the results for the ethanol process are presented based on the ethanol/water mixture that exits the fermentation reactor.

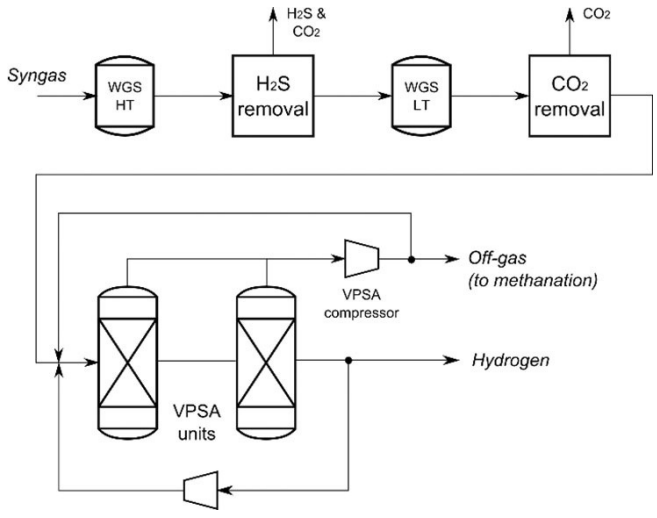

Figure 5. VPSA design scheme (syngas from the COS reactor and heat exchangers and condensers not included).

Vacuum pressure swing adsorption (VPSA)

A VPSA[47,54] unit for hydrogen separation is selected to minimize electricity consumption, if we consider the pressure levels in the process. The hydrogen stream is delivered at 13.1 bar without supplementary compression. Instead, the remaining methane-rich gas is recompressed from 0.8 to 7.5 bar before the final methanation stages.

The VPSA is controlled to allow separation of 75–95 %[47] of the hydrogen in the syngas stream and to have a H_2/CO ratio in the remaining gas stream that matches the requirement for methanation. In the coproduction of hydrogen and methane, the electricity demand in the plant can be a limiting factor because of the increased consumption by the VPSA compressor and the different heat releases in the methanation reactors. Therefore, for design D, we investigated two cases, $zero_{El}$ and max_{H_2}, in which H_2 production is controlled so as to have a zero consumption of electricity in the plant in the first case, and in the second case, electricity from the grid is used to maximize H_2 production. The maximum hydrogen production level is obtained by increasing the WGS and the hydrogen separation in the VPSA system up to the maximum level of 95 %.

STG and methane coproduction

During the production of STG, the excess heat in the process may be insufficient to cover the heat demand of the dryers and for the generation of electricity because of the absence or reduction of the methanation reaction. Therefore, the simulation was performed for two cases: (i) $zero_{El}$, in which combustion is increased to provide heat for the steam cycle to cover the internal electricity demand of the plant and (ii) max_{STG}, in which the DFB gasifier is operated as shown in design A.3 LT and electricity is bought from the grid.

Heat integration and steam cycle

Here, the ideal heat recovery targets are estimated from the analysis of the thermal cascade of the process by setting a minimum temperature difference (ΔT_{min}) for heat exchange and by applying the pinch analysis in line with previous studies.[30,55] The grand composite curves (GCC) are used to represent the heat cascade graphically, which shows the amounts of heat available in the process at the different temperature levels for conditions of ideal heat recovery. To investigate the integration of the steam cycle in the process, the GCC of the process and the steam cycle are plotted against each other by applying the principles of split-GCC graphical analysis.[30]

To optimize the steam cycle steam temperature and pressure levels, the optimal mass flows to maximize the power production are predefined. In the steam cycle, the steam data at the first stage of the turbine are set as constant for all the designs, whereas the other pressure levels are varied depending on the temperature levels in the heat cascade. District heating is not included in the study, and a water stream at 15 °C is used as the cold utility. The isentropic efficiency of the turbine $\eta_{T,is}$ is in the range of 0.78–0.93 and is estimated as a function of mass flow and pressure [Eqs. (5)–(7)], based on previous work.[56] The data used in the steam cycle are summarized in Table 4.

$$\eta_{T,is} = 0.0517\ln(x) + 0.515 \text{ for } x < 500 \quad (5)$$

$$\eta_{T,is} = 0.035\ln(x) + 0.622 \text{ for } x < 500 \quad (6)$$

$$x = \frac{m\ \dot{\Delta}h_{is}}{P_1 - P_2} \quad (7)$$

Process indicators

The performance analysis of a multiproduct plant requires the monitoring of several streams and it can be evaluated by different efficiencies. The evaluation of the outlet streams in this work includes all the chemical products (biomethane, STG, hydrogen, and ethanol) as well as the CO_2 streams for potential carbon storage or other applications. The chemical efficiency η_{ch} (Table 5) is calculated from the yields of chemical products based on the sole biomass energy input. Notably, the efficiency of ethanol production is given on a dry basis and the energy penalty for the distillation is not considered, as discussed above. The electricity in the plant can be produced and delivered to the grid or consumed from the grid; in the definitions of the efficiencies, this is described by the net electricity consumption El_{in} and the net production of electricity El_{out}. The performance of the gasification section is evaluated by the cold gas efficiency η_{CG}, calculated as the energy content in the product gas compared to the energy in the dry as free biomass.

The chemical and total efficiencies (Table 5) can be calculated from the energy input of the biomass (η_{ch}, η_{tot}) or the total energy input that includes the RME flow (η^*_{ch}, η^*_{tot}). In the results, the efficiencies are calculated from the lower heating value of the as-received biomass ($LHV_{a.r.}$) with 50 % w.b. moisture, which corresponds to the average moisture content after harvesting in the northern hemisphere. This biomass is of the lowest market value, which is critical for the economic viability of the plant; further drying to 40 % moisture is assumed to occur naturally if sufficient storage time is allowed before delivery. The results based on the LHV_{daf} are reported for comparison with other studies and are comparable with the efficiencies calculated from the higher heating value (HHV).

The power-to-gas conversion is assessed based on the efficiency η_{P2G}, which is a marginal efficiency that compares the increment of biomethane production from a reference case with the amount of electricity consumed to obtain that increment. This is not an absolute value as it depends on the reference process.

Table 5. Efficiency definitions.

Efficiency	Definition
	based on biomass input
cold gas efficiency	$\eta_{CG} = \frac{E_{CG}}{E_{biom}}$
chemical efficiency	$\eta_{ch} = \frac{E_{CH_4} + E_{STG} + E_{H_2} + E_{ethan}}{E_{biom}}$
total efficiency	$\eta_{tot} = \frac{E_{CH_4} + E_{STG} + E_{H_2} + E_{ethan} + El_{out}}{E_{biom} + El_{in}}$
power-to-gas efficiency	$\eta_{P2G} = \frac{E_{CH_4} - E'_{CH_4}}{El_{in} - E'_{out}}$
	based on all energy inputs
chemical efficiency	$\eta^*_{ch} = \frac{E_{CH_4} + E_{STG} + E_{H_2} + E_{ethan}}{E_{biom} + E_{RME}}$
total efficiency	$\eta^*_{tot} = \frac{E_{CH_4} + E_{STG} + E_{H_2} + E_{ethan} + El_{out}}{E_{biom} + El_{in} + E_{RME}}$

['] Reference process, as in equations.

Results and Discussion

The gas compositions calculated for different stages of the process and the error levels compared to the data obtained from the GoBiGas plant are given in Table 6. The calculation

Table 6. Validation of the model versus measurements from the GoBiGas plant (A.1 HT design). The equipment numbers refer to Figure 3.

Outlet reactor	6	7	11	13	15	17	18	Final
H_2 [$\%_v$]	41.8	41.8	41.8	40.5	47.9	35.3	48.3	1.9
CO [$\%_v$]	23.7	23.7	23.7	24.3	28.5	11.5	14.4	≈0
CO_2 [$\%_v$]	24.9	24.9	24.9	25.3	12.0	26.4	1.7	1.1
CH_4 [$\%_v$]	7.6	7.6	7.6	7.8	9.2	26.8	35.6	97
C_2H_4 [$\%_v$]	2.0	2.0	2.0	0	0	0	0	0
C_3H_6 [$\%_v$]	≈0	≈0	≈0	0	0	0	0	0
C_2H_6 [$\%_v$]	0	0	0	2.1	2.4	≈0	≈0	≈0
C_3H_8 [$\%_v$]	0	0	0	≈0	≈0	≈0	≈0	0
H_2S [ppm]	≈100	≈100	<5	<5	0	0	0	0
BTX [g Nm^{-3}]	7	7	0	0	0	0	0	0
C_7H_{10} [g Nm^{-3}]	13.5	0	0	0	0	0	0	0

Table 7. Results of the simulated designs for a biomass input of 100 MW_{daf} and RME input of 3.3 MW_{RME}. The designs and cases are described in the Methodology and Process layout and modeling sections.

Material products	Design A.1 no drying			Design A.2 air-drying		Design A.3 base case		Design A.4 (LT) electrolysis		Design A.5 (LT) direct heating		Design B (LT) ethanol + CH_4		Design C (LT) STG		Design D (LT) H_2 + CH_4	
	HT	LT	750 °C	HT	LT	HT	LT	$zero_{EI}$	max_{EI}	$zero_{EI}$	max_{EI}	$c_{80\%}$	$c_{50\%}$	$zero_{EI}$	max_{STG}	$zero_{EI}$	max_{H_2}
biomethane [MW_{CH_4}]	56.8	57.6	61.3	67	67.9	71.2	72.0	72.8	80.4	73.4	77.2	42.5	49.1	0	0	51	35.6
ethanol [$t\,h^{-1}$][a]	0			0	0	0	0	0	0	0	0	3.41	2.69	0	0	0	0
STG [MW_{STG}][b]	0			0	0	0	0	0	0	0	0	0	0	85.6	91.6	0	0
hydrogen [MW_{H_2}]	0			0	0	0	0	0	0	0	0	0	0	0	0	22.5	42.4
separated CO_2 [$t\,h^{-1}$][c,d]	14.3	15.4	16.0	15.9	16.3	16.4	16.4	16.3	15.4	16.5	17	10.1	10.8	7.1	7.1	20.0	23.3
electricity balance																	
$El_{out}-El_{in}$ [MW_{el}]	6.2	4.7	3.0	3.2	2.4	1.6	1.2	≈0	−12.8	≈0	−3.4	≈0	≈0	≈0	−3.8	≈0	−6.1
El_{demand} [MW_{el}]	4.1	4.1	4.3	4.8	4.7	5.4	5.3	7.1	20.5	7.0	10.5	4.3	4.7	4.5	4.8	6.2	12.1
compressor [MW_{el}]	2.9	2.9	3.0	3.2	3.2	3.4	3.4	3.4	3.5	3.5	3.8	1.6	2.6	3.2	3.4	3.3	3.4
dryers [MW_{el}]				0.35	0.35	0.8	0.8	0.8	0.8	0.8	0.8	0.8	0.8	0.80	0.80	0.8	0.8
El_{P2G} [MW_{el}]								1.2	15	1.2	4.8						
LT heat demands																	
$Q_{reboilers}$ [MW][e]	5.2	5.6	5.8	5.8	6.0	6.1	6.1	6.0	5.6	6.0	6.3	5.1[e]	5.2[e]	2	2.1	7.3	10.0
Q_{dryers} [MW]				6.1	6.1	8.9	8.9	8.9	8.9	8.9	8.9	8.9	8.9	8.9	8.9	8.9	8.9
fuel conversion																	
char gasification	0.4	0.4	0.4	0.45	0.53	0.56	0.61	0.61	0.61	0.6	0.7	0.61	0.61	0.48	0.61	0.58	0.61
recirc. of raw gas [MW]	10.1	4.4	0.9	0.9	0.9	0.9	0.9	0.9	0.9	0.9	0.9	0.9	0.9	0.9	0.9	0.9	0.9
efficiencies																	
η_{CG} [% LHV_{daf}]	67.4	68.1	72.3	79.2	79.8	84.0	84.8	85.7	94.7	86.7	91.0	84.8	84.8	84.8	84.8	84.8	84.8
η_{ch} [% LHV_{daf}]	56.8	57.6	61.3	67	67.9	71.2	72	72.8	80.4	73.4	77.2	67.9	69.1	85.6	91.6	73.5	78
η_{tot} [% LHV_{daf}]	63	62.3	64.3	70.2	70.3	72.8	73.2	72.8	70.5	73.4	73.8	69.7	71.1	85.6	88.2	73.5	73.6
η_{ch} [% $LHV_{a.r.}$][f]	65.3	66.3	70.5	77.1	78	81.9	82.8	83.8	92.5	84.4	88.8	78.1	79.5	98.5	105.4	84.6	89.7
η_{tot} [% $LHV_{a.r.}$][f]	72.5	71.7	73.6	80.8	80.9	83.8	84.2	83.8	81.1	84.4	85.0	80.2	81.8	98.5	101.5	84.6	84.7
η_{P2G} [%]								65[g]	60[g]	118[g]	114[g]				158[h]		74[i]

[a] In solution with water ≈5 $g\,L^{-}$. [b] After H_2S removal. [c] Net of the purge gas. [d] Contains H_2S. [e] No distillation. [f] Based on 50% w.b. moisture biomass. [g] Reference design A.3 LT. [h] Reference design C $zero_{EI}$. [i] Reference design D $zero_{EI}$.

shows a deviation from the measurements made at the plant in the range of ±10%. Therefore, the flow-sheet model is considered to be reliable for simulations. The results for each design are presented in Table 7, and the production and efficiency ranges and the rates of conversion of electricity to biofuels are compared in Figures 6 and 7.

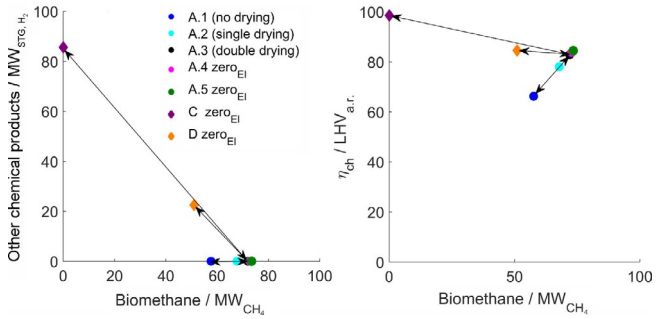

Figure 6. Production ranges of the investigated plant designs.

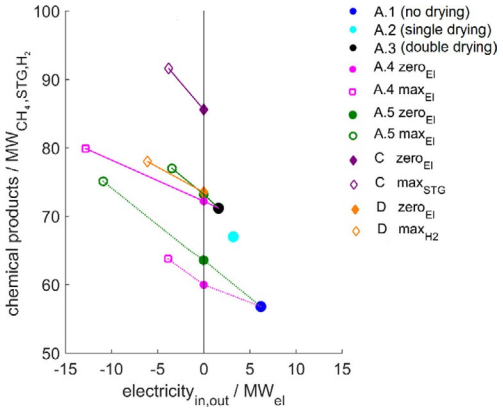

Figure 7. Chemical production versus electricity consumption for plant designs that involve the conversion of electricity to bioproducts. The filled symbols indicate net electricity production level equal to or higher than zero.

Influences of drying and operational conditions of the gasifier

The evaluation of the standalone biomethane designs A.1–A.3 was performed with high-temperature (HT) and low-temperature (LT) operational conditions (Table 7). A comparison of designs A.1, A.2, and A.3 shows that the integration of a drying system in the plant is the parameter that exerts the strongest effect on the chemical efficiency and biomethane production as the variation of the moisture content of the fuel affects the heat balance of the DFB gasifier directly. A major improvement is achieved if we move from design A.1 to design A.2, that is, if we introduce an air dryer (to reduce the moisture content from 40 to 20% w.b.), which corresponds to an increase in cold gas efficiency of the gasifier of around 12 percentage points (pp) and of the chemical efficiency of around 10 pp to reach 78% $LHV_{a.r.}$. The higher level of methane production is counterbalanced by the slight-

ly lower production of electricity. The increment in production related to the presence of a first drying stage would justify its introduction in any new plant. The introduction of a steam dryer with moisture recovery is more susceptible to the high cost of installation, whereas the advantage on η_{ch} is quantified to be approximately 4% to achieve a chemical efficiency of 82.8% $LHV_{a.r.}$ for design A.3 LT.

The improvements in relation to the GoBiGas demonstration plant (η_{ch} estimated at 57.4% $LHV_{a.r.}$[22]) if different drying strategies are introduced are shown in Figure 6. Here, the gap between designs A.2 and A.3 could be considered as the performance expected for a large-scale standalone plant.

The decrease of the gasification temperature from the HT to the LT case would increase the chemical efficiency of the plant by around 0.8%, which corresponds roughly to the decrease in the internal heat demand of the gasifier. Ongoing research on the catalytic effects of the ash compounds on tar chemistry has revealed the potential to decrease the temperature in the DFB reactor even further.[57] An extrapolation exercise with a gasification temperature of 750 °C and with the same tar content as that under LT conditions but with a decrease of the char gasification to 40% was performed for design A.1 and showed a further improvement in η_{ch} of 3.7%. However, lower temperatures in the reactor are unfavorable for char gasification, which could lead to a level of char conversion that is not feasible for a real process.

Coproduction of biomethane and ethanol

The results obtained for the coproduction of ethanol and biomethane are shown in Table 7 and Figures 6 and 7, in which $c_{80\%}$ and $c_{50\%}$ indicate the cases with rates of conversion of CO up to 80 and 50%, respectively. The yield of ethanol is reported as a mixture with water (with a concentration of $\approx 5\,g\,L^{-1}$). However, a strategy for distillation that involves other low-temperature sources should be incorporated to make this design interesting, otherwise the heat demand for distillation will decrease the chemical efficiency of the plant considerably. The values reported in Table 7 represent the maximum levels of ethanol production achieved by operating the ethanol plant upstream of the methanation section. The maximum production of ethanol is estimated to range from 3.41 ($c_{80\%}$ case) to $2.69\,t\,h^{-1}$ ($c_{50\%}$ case) with coproduction levels of 42.5 and 49.1 MW_{CH_4}, respectively. The production of biomethane can be increased by using a partial bypass of the ethanol plant to achieve up to 100% biomethane (Figure 6).

Drop-in gasification plants for STG and hydrogen production

The simulation of design C is performed for two separate cases: the first, $zero_{El}$, with a STG production of 85.6 MW_{STG}; and the second, max_{STG}, with a maximum production of 91.6 MW_{STG} and an electrical consumption of 3.8 MW_{el}. The composition of the STG resembles that of the raw gas (and is, therefore, dependent upon the operation of the gasifier), with a H_2/CO ratio of approximately 2, methane content if 8%$_v$, and CO_2 content of approximately 12%$_v$. The production of STG has the advantage that it retains the high efficiency of the gasification process because of the minimum requirement of conditioning the gas products. The chemical efficiency of the $zero_{El}$ case is 98% $LHV_{a.r.}$ and it increases to 105.4% $LHV_{a.r.}$ for the max_{STG} case with a total efficiency of 101.5% $LHV_{a.r.}$ ($El_{in} = 3.8\,MW_{el}$).

In addition, the coproduction of hydrogen and methane (design D) is investigated for two cases: $zero_{El}$ and max_{H_2}, in which electricity obtained from the grid is used to maximize H_2 production. In the $zero_{El}$ case, the production levels of H_2 and CH_4 are 22.5 MW_{H_2} and 51 MW_{CH_4} and the chemical efficiency is 84.6% $LHV_{a.r.}$. In the max_{H_2} case, H_2 production is increased to 42.4 MW_{H_2} with a methane production level of 35.6 MW_{CH_4} and an electricity consumption of 6.1 MW_{el}. The chemical efficiency of the plant increases if it changes from exclusively CH_4 production to H_2, although it does not reach the efficiency level seen for STG production (Figure 6b).

Comparison of power-to-gas concepts

Direct heating and electrolysis power-to-gas technologies are investigated in designs A.5 and A.4 based on design A.3. For both A.5 and A.4, two cases are investigated: a $zero_{El}$ case and a maximum electricity case max_{El}. The power-to-gas efficiency is higher for direct heating ($\eta_{P2G} \approx 115\%$), whereas electrolysis achieves an efficiency of $\eta_{P2G} \approx 63\%$. However, the two power-to-gas technologies exhibit different ranges of operation, which depend on the initial design of the plant. In particular, the application of direct heating is quite limited in design A.3 (max_{El} case: $El_{in} = 3.4\,MW_{el}$ and $El_{P2G} = 4.8\,MW_{el}$) as char gasification is already close to the maximum value; instead, electrolysis is favored by the high carbon yield in the raw gas and the conversion range was higher (max_{El} case: $El_{in} = 15\,MW_{el}$ and $El_{P2G} = 12.8\,MW_{el}$). This trend is reversed if these power-to-gas technologies are applied to design A.1, in which direct heating first reduces the product gas recirculation and then leads to an increase in char gasification.

The electricity demand/production and the chemical production of the plants for the two power-to-gas technologies and the other designs that offer the possibility to convert electricity into bioproducts are shown in Figure 7, as in design C (max_{STG} case) and design D (max_{H_2} case). In particular, the power-to-gas efficiency of the overall STG process (calculated using the $zero_{El}$ case as a reference) is even higher than that of direct heating (Table 7), as obtaining the electricity from the grid avoids the combustion of char or product gas for electricity generation, which thereby increases the production of STG. Therefore, electricity can be converted to bioproducts in standalone biomethane plants or distributed drop-in STG plants with similar performance levels. Notably, the maximum chemical efficiency for a standalone plant is achieved for designs A.4 $zero_{El}$ at 84.4% $LHV_{a.r.}$, which represents the maximum efficiency for a conversion of 50% w.b. moisture biomass to biomethane.

Aspects of heat integration

The heat integration in the plant is crucial to achieve high efficiencies. In particular, the use of medium-/low-temperature heat in the dryers and high-temperature heat in the preheaters is important to optimize the heat balance of the DFB gasifier to achieve a high conversion efficiency. In general, the process can be optimized to become self-sustaining by using excess heat from the exothermic steps to maximize the syngas production (chemical efficiency) and to produce some electricity (designs A.1–5, C zero$_{El}$, D zero$_{El}$).

However, all the designs exhibit a heavy demand for low-temperature heat because of the drying step, and the reboilers connected to the H_2S and CO_2 separation steps and the process could benefit from external low-temperature heat sources, such as industrial processes in the vicinity or pulp mills and existing (CHP) plants (local heat integration).

The effect of other low-temperature heat sources can be quantified as an increase in electricity production as shown in Figure 8, in which the GCC for the A.3 (LT) design are plotted together with the corresponding curve obtained after removing the heat demands below 160 °C (≈22.5 MW$_{th}$).

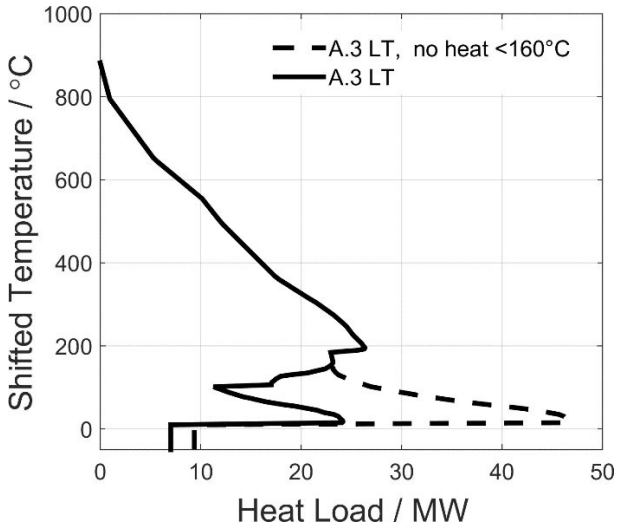

Figure 8. GCC for design A.3 that shows the integration of the steam cycle and biomethane process (which includes cold utility).

The effect is an increase in electricity production in the steam cycle from 6.5 to 9.4 MW$_{el}$. For ethanol coproduction, the opportunity to use excess heat from other processes is crucial to ensure the profitably of the plant as it can be used for distillation, which preserves the high efficiency of the gasification process.

CO_2 as a product

The amounts of CO_2 separated for the investigated plant designs are shown in Figure 9. As expected, design D stands out as having a strong potential to separate the used carbon on-site. Designs A.1–A.3 have similar potentials in which the CO_2 production that increases linearly leads towards higher

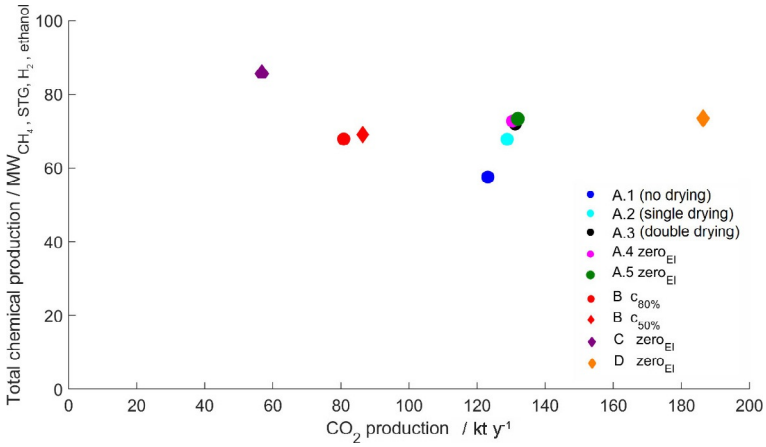

Figure 9. Production ranges of CO_2 as a function of chemical production in the investigated plant designs.

yields of CH_4. The amount of CO_2 produced at the gasification plant (in the range of 57–186 kt yr^{-1}; cf. Figure 9) is at the low end of what is generally considered feasible for CCS.[34] However, the geographical location of the plant, specifically if it is in proximity to a coastline as well as a harbor and if it is part of an industrial cluster, facilitates the implementation of CCS at the gasification plant.

Conclusions

The production ranges and efficiencies are compared between distributed drop-in and centralized drop-in plants and standalone plants for biomass gasification based on dual fluidized bed (DFB) technology. Two intermediate semiproducts for distribution from distributed drop-in and centralized drop-in plants are considered: sustainable town gas (STG; a mixture of CO, H_2, CO_2, and CH_4) and pure H_2 in combination with pure biomethane. The investigation uses the 32 MW$_{biomass}$ standalone GoBiGas plant as reference to consider the scale-up of the technology to 100 MW$_{biomass}$. Measures to improve the efficiency that become feasible at larger scales are investigated, which includes an advanced drying system for the biomass, different operation of the gasifier, and power-to-gas strategies. The considered feedstock is biomass 50 % wet basis (w.b.) moisture, which is dried naturally to 40 % w.b. before it undergoes conversion in the plant.

Our results show that it is possible for standalone plants to increase the chemical efficiency from the current level of 57.4 lower heating value of the as-received biomass (% LHV$_{a.r.}$)[22] to levels within the range of 78–82.8 % LHV$_{a.r.}$.

With large-scale deployment, distributed drop-in and centralized drop-in plants can achieve chemical efficiencies in the ranges of 82.8–98.5 % $LHV_{a.r.}$ for STG/biomethane and 82.8–84.6 % $LHV_{a.r.}$ for H_2/biomethane. The production range for STG/biomethane production ranges from 85.6 MW_{STG} (design C $zero_{El}$) to 72 MW_{CH_4} (design A.3) and for H_2/biomethane it ranges from 22.5 MW_{H_2} and 51 MW_{CH_4} (design D $zero_{El}$) to 72 MW_{CH_4} (design A.3). As a result of the high efficiency levels and the extended range of convenient locations for distributed drop-in and centralized drop-in plants, there is no substantial advantage associated with standalone plants that produce biomethane, unless methane is the desired final product.

The potential of power-to-gas technologies in gasification plants was investigated for standalone plants and compared with the use of electricity to increase production levels in distributed and centralized drop-in plants. The results for the standalone plants show that the direct heating of the DFB gasifier gives a higher conversion efficiency than an electrolysis process, that is, approximately 115 % compared to approximately 63 %. However, the amount of electricity that can be converted into energy bound chemically by direct heating is limited by the rate of char gasification in the gasifier. Thus, in process designs that involve extensive drying (design A.3), the range of applications of direct heating is more limited than electrolysis, and the opposite holds true for designs with low (or zero) drying (design A.1). In distributed drop-in plants, electricity from the grid can be used to boost the chemical production process, which increases the maximum production of STG to 91.6 MW_{STG} (design C max_{STG}) and of H_2 to 42.4 MW_{H_2} (design D max_{H_2}), with power-to-gas efficiencies comparable to or higher than the power-to-gas technologies in standalone plants.

Overall, DFB gasification plants show good flexibility in relation to product output and retain a high efficiency if drying is implemented and heat integration in the plant is optimized. Further economic investigations of the local context are necessary to define introduction strategies for new gasification plants. However, the results of the present study show that distributed and centralized drop-in strategies can be as profitable as or more profitable than standalone biomethane plants, such that they should be considered in an analysis of the local energy system.

Acknowledgements

This work was performed within the Competency Center of Svenskt Förgasningscentrum (SFC), in collaboration with the Swedish Energy Agency and Göteborg Energi. The authors would like to acknowledge the collaboration of Matteo Morandin, Chalmers University of Technology.

Keywords: biomass · biomethane · gobigas · hydrogen · power-to-gas

[1] C. H. Zhou, X. Xia, C. X. Lin, D. S. Tong, J. Beltramini, *Chem. Soc. Rev.* **2011**, *40*, 5588–5617.
[2] L. H. Zhang, C. B. Xu, P. Champagne, *Energy Convers. Manage.* **2010**, *51*, 969–982.
[3] M. Hoogwijk, A. Faaij, B. Eickhout, B. de Vries, W. Turkenburg, *Biomass Bioenergy* **2005**, *29*, 225–257.
[4] V. S. Sikarwar, M. Zhao, P. Clough, J. Yao, X. Zhong, M. Z. Memon, N. Shah, E. J. Anthony, P. S. Fennell, *Energy Environ. Sci.* **2016**, *9*, 2939–2977.
[5] J. Hrbek, *Status report on thermal biomass gasification in countries participating in IEA Bioenergy*, *Task 33*, www.ieabioenergytask33.org, **2016**.
[6] H. Hofbauer, R. Rauch, K. Bosch, R. Koch, C. *APCBEE Procedia*, **2003**, 527–536.
[7] A. Larsson, M. Hedenskog, H. Thunman, presented in part at the *Nordic Flame Days*, Copenhagen, **2015**.
[8] A. Larsson, M. Seemann, D. Neves, H. Thunman, *Energy Fuels* **2013**, *27*, 6665–6680.
[9] Biomass CHP station Senden, http://www.4biomass.eu/en/best-practice/project-biomass-chp-station-senden.
[10] S. Heyne, H. Thunman, S. Harvey, *Int. J. Energy Res.* **2012**, *36*, 670–681.
[11] H. Holmberg, P. Ahtila, *Appl Therm Eng.* **2005**, *25*, 3115–3128.
[12] M. Gassner, F. Marechal, *Energy Environ. Sci.* **2012**, *5*, 5768–5789.
[13] M. Gassner, F. Marechal, *Biomass Bioenergy* **2009**, *33*, 1587–1604.
[14] T. R. Brown, R. C. Brown, *RSC Adv.* **2013**, *3*, 5758–5764.
[15] W. N. Zhang, *Fuel Process. Technol.* **2010**, *91*, 866–876.
[16] C. M. van der Meijden, H. J. Veringa, L. Rabou, *Biomass Bioenergy* **2010**, *34*, 302–311.
[17] P. N. Vennestrøm, C. M. Osmundsen, C. H. Christensen, E. Taarning, *Angew. Chem. Int. Ed.* **2011**, *50*, 10502–10509; *Angew. Chem.* **2011**, *123*, 10686–10694.
[18] I. Hannula, V. Arpiainen, *Biomass Convers. Biorefin.* **2015**, *5*, 63–74.
[19] H. Boerrigter, R. Rauch, *Review of applications of gases from biomass gasification Energy Research of the Netherlands (ECN)*, **2006**.
[20] H. Thunman, A. Larsson, M. Hedenskog, Commissioning of the GoBiGas 20MW plant biomethane plant. Conference:TCBiomass **2015** Chicago, **2015**.
[21] M. Karlbrink, Master of Science Thesis, Chalmers University of Technology, Gothenburg, **2015**.
[22] A. Alamia, A. Larsson, C. Breitholtz, H. Thunman, *Int. J. Energy Res.* **2017**, accepted.
[23] I. Gunnarsson, *The GoBiGas project*, **2011**.
[24] G. Aranda, A. van der Drift, R. Smit, *The Economy of Large Scale Biomass to Substitute Natural Gas (bioSNG) plants*, *Energy Research of the Netherlands (ECN)*, **2014**.
[25] A. L. Soerensen, *Economies of Scale in Biomass Gasification Systems*, *International Institute for Applied Systems Analysis (IIASA)*, **2005**.
[26] R. M. Handler, D. R. Shonnard, E. M. Griffing, A. Lai, I. Palou-Rivera, *Ind. Eng. Chem. Res.* **2016**, *55*, 3253–3261.
[27] J. Daniell, M. Kopke, S. D. Simpson, *Energies* **2012**, *5*, 5372–5417.
[28] H. Holmberg, P. Ahtila, *Biomass Bioenergy* **2004**, *26*, 515–530.
[29] A. Alamia, H. Thunman, M. Seemann, *Energ Fuel.* **2016**, *30*, 4017–4033.
[30] I. Kemp, *Pinch Analysis and Process Integration*, 2nd ed., Elsevier, Oxford, **2007**.
[31] M. K. Bora, S. Nakkeeran, *Int. J. Adv. Res.* **2014**, *2*, 561–574.
[32] M. Bolhàr-Nordenkampf, A. Friedl, U. Koss, T. Tork, *Chem. Eng. Process.* **2004**, *43*, 701–715.
[33] C. Azar, D. J. A. Johansson, N. Mattsson, *Environ. Res. Lett.*, **2013**, *8*, 034004.
[34] J. Kjärstad, R. Skagestad, N.-H. Eldrup, F. Johnsson, *Int. J. Greenhouse Gas Control* **2016**, *54*, 168–184.
[35] H. Topsøe, *From solid fuels to substitute natural gas (SNG) using TREMP™*, **2009**.
[36] H. Topsøe, *From Coal to Clean Energy*, file:///D:/Users/alamia.NET/Downloads/topsoe_from_coal_to_clean_energy_nitrogen_syngas_march_april 2011.pdf.
[37] A. Alamia, H. Ström, H. Thunman, *Biomass Bioenergy* **2015**, *77*, 92–109.

[38] K. P. Brooks, J. Hu, H. Zhu, R. J. Kee, *Chem. Eng. Sci.* **2007**, *62*, 1161–1170.
[39] S. K. Hoekman, A. Broch, C. Robbins, R. Purcell, *Int. J. Greenhouse Gas Control* **2010**, *4*, 44–50.
[40] M. Götz, J. Lefebvre, F. Mörs, A. McDaniel Koch, F. Graf, S. Bajohr, R. Reimert, T. Kolb, *Renewable Energy* **2016**, *85*, 1371–1390.
[41] Pressure Electrolyser, http://elektrolyse.de/wordpress/?page_id=38.
[42] A. J. Appleby, G. Crepy, J. Jacquelin, *Int. J. Hydrogen Energy* **1978**, *3*, 21–37.
[43] J. Marinkovic, H. Thunman, P. Knutsson, M. Seemann, *Chem. Eng. J.* **2015**, *279*, 555–566.
[44] K. Liu, H. K. Atiyeh, R. S. Tanner, M. R. Wilkins, R. L. Huhnke, *Bioresour. Technol.* **2012**, *104*, 336–341.
[45] M. Köpke, C. Mihalcea, J. C. Bromley, S. D. Simpson, *Curr. Opin. Biotechnol.* **2011**, *22*, 320–325.
[46] F. R. Bengelsdorf, M. Straub, P. Durre, *Environ. Technol.* **2013**, *34*, 1639–1651.
[47] D. Johansson, P. A. Franck, T. Berntsson, *Energy* **2012**, *38*, 212–227.
[48] P. C. Munasinghe, S. K. Khanal, *Bioresour. Technol.* **2010**, *101*, 5013–5022.
[49] K. Liu, H. K. Atiyeh, B. S. Stevenson, R. S. Tanner, M. R. Wilkins, R. L. Huhnke, *Bioresour. Technol.* **2014**, *151*, 69–77.
[50] LanzaTech, *Aemetis Acquires License from LanzaTech with California Exclusive Rights for Advanced Ethanol from Biomass*, http://www.lanzatech.com/aemetis-acquires-license-lanzatech-california-exclusive-rights-advanced-ethanol-biomass-including-forest-ag-wastes/.
[51] J. He, W. N. Zhang, *Appl Energ.* **2011**, *88*, 1224–1232.
[52] C. Piccolo, F. Bezzo, *Biomass Bioenergy* **2009**, *33*, 478–491.
[53] J. R. Phillips, E. C. Clausen, J. L. Gaddy, *Appl. Biochem. Biotechnol.* **1994**, *45*, 145–157.
[54] M. T. Ho, G. W. Allinson, D. E. Wiley, *Ind. Eng. Chem. Res.* **2008**, *47*, 4883–4890.
[55] B. Linnhoff, D. W. Townsend, D. Boland, G. F. Hewitt, B. E. A. Thomas, A. R. Guy, R. H. Marsland, *User Guide on Process Integration for the Efficient Use of Energy*, 1st ed., **1982**.
[56] T. Savola, K. Keppo, *Appl. Therm. Eng.* **2005**, *25*, 1219–1232.
[57] T. Berdugo Vilches, "Strategies for controlling solid biomass conversion in dual fluidized bed gasifiers" Licentiate engineer thesis, Chalmers University of Technology, Gothenburg, **2016**.

Manuscript received: November 17, 2016
Revised manuscript received: December 22, 2016
Accepted manuscript online: December 28, 2016
Version of record online: April 4, 2017

